AJNR

Intracranial ependymoma and subependymoma: MR manifestations.

G P Spoto, G A Press, J R Hesselink and M Solomon

AJNR Am J Neuroradiol 1990, 11 (1) 83-91
http://www.ajnr.org/content/11/1/83

Intracranial Ependymoma and Subependymoma: MR Manifestations

Gary P. Spoto[1]
Gary A. Press[1]
John R. Hesselink[1]
Murray Solomon[2]

In order to provide a detailed description of the MR appearance of intracranial ependymoma, the MR examinations of 12 patients (10 with ependymomas and two with subependymomas) were reviewed and correlated with operative and pathologic reports. Three of 10 ependymomas were intraventricular, two were intraparenchymal, and five were transependymal, extending from CSF spaces into parenchyma. Both subependymomas were intraventricular. Solid ependymomas and subependymomas were iso- to hypointense relative to normal white matter on T1-weighted images and hyperintense on proton-density- and T2-weighted images. Foci of signal heterogeneity within solid neoplasms represented methemoglobin, hemosiderin, necrosis, calcification, and encased native vessels or tumor vascularity. Gd-DTPA–enhanced images in two patients differentiated enhancing tumor from surrounding nonenhancing edema and from surrounding normal brain parenchyma. Cystic neoplasms had sharply defined, round or oval margins and uniform signal intensity equivalent to or slightly hyperintense relative to CSF. Tumor-associated calcification was not demonstrated readily by MR. Sagittal and coronal images were valuable in assessing the amount of intraventricular tumor and route of extension.

We conclude that the MR differentiation of ependymomas and subependymomas from other gliomas is provided most reliably by the location and morphology of the tumor and not by differences in signal intensity. The typical ependymoma arises within the fourth ventricle as a solid mass with heterogeneous signal intensity. A propensity for spread is seen along the CSF pathways via the foramina of Magendie and Luschka and the aqueduct of Sylvius. Supratentorial ependymomas may be periventricular in location and have cystic components. The two subependymomas in our series were solid, intraventricular tumors with relatively homogeneous signal intensities.

***AJNR* 11:83–91, January/February 1990; *AJR* 154: April 1990**

The appearance of intracranial ependymoma and subependymoma, although well characterized on CT [1–3], has not been described in detail on MR. To our knowledge, the MR findings of ependymoma have been reported in only a few cases, as part of larger series of intracranial neoplasms [4–8]; there is only one prior report on the MR manifestations of subependymoma [9].

We correlated the MR findings with operative and pathologic reports in 10 patients with proved intracranial ependymomas and two patients with subependymomas. The appearance of ependymoma at low (0.35 T) and high (1.5 T) field strengths is described.

Materials and Methods

We reviewed 14 MR studies of 10 patients with intracranial ependymomas and two patients with subependymomas. The operative and pathologic reports and hospital and outpatient records were available for all but two patients; these clinical data were correlated with the MR findings. The patients ranged in age from 1.2 to 59.0 years (mean, 23.6 years). There were six females and six males. MR examinations performed at initial presentation were

Received January 25, 1989; revision requested March 29, 1989; revision received June 29, 1989; accepted July 10, 1989.

[1] Department of Radiology and Magnetic Resonance Institute, University of California, San Diego, School of Medicine, 225 Dickinson St., San Diego, CA 92103. Address reprint requests to G. A. Press.

[2] Los Gatos MRI Center, 800 Pollard Rd., Los Gatos, CA 95030.

0195-6108/80/1101-083

available in seven patients. Two of these patients were imaged again postoperatively (Table 1); one (case 7) was reexamined 12 days after surgical debulking; the other (case 4) was restudied at the time of recurrence, 11 months after surgery. In the other five patients, MR was performed at the time of recurrence. Nine examinations were performed at 1.5 T; five studies were performed at 0.35 T.

Spin-echo images acquired at 1.5 T (General Electric, Milwaukee) were 3–5 mm thick and usually had a 256 × 256 matrix. In one examination (case 6), a 128 × 128 matrix was used in one sequence; in two others (cases 1 and 7) a rectangular pixel (256 × 128 matrix) was used in some sequences. Consecutive slices were separated by a 1.0- or 2.5-mm gap. T1-weighted images, 600–900/20–25/2 (TR/TE/excitations), proton-density-weighted images, 1500–3000/20–35/2, and T2-weighted images, 1500–3000/60–80/2, were obtained in all patients. The sequences with a rectangular pixel used only one excitation. Images were acquired in the axial plane in each examination (T1-weighted in four, proton-density, and T2-weighted in eight); sagittal images were obtained in eight studies (T1-weighted in eight, proton-density- and T2-weighted in one); coronal proton-density and T2-weighted images were obtained in two examinations. Gadolinium-DTPA (Gd-DTPA)–enhanced images were obtained in two patients (cases 7 and 11). In case 7, Gd-DTPA was administered during the postoperative MR examination only.

MR images acquired at 0.35 T (Diasonics, San Francisco) were 10 mm thick and had a 256 × 256 matrix in all cases. Consecutive slices were separated by a 0- or 1.0-mm interslice gap. T1-weighted images (500/28–30/2) were obtained in four examinations; a TR of 1000 was used in one study. Proton-density-weighted (1500–2500/28–30/2) and T2-weighted (1500–2500/56–60/2) images were acquired in each examination. One examination included a partial-flip-angle sequence, 500/30/30° (TR/TE/flip angle). In addition to axial images acquired in each study (T1-weighted in four, proton-density- and T2-weighted in four), sagittal images were obtained in three (T1-weighted in two, proton-density- and T2-weighted in two) and coronal images were obtained in two examinations (proton-density-weighted in two and T2-weighted in one).

CT (General Electric 9800, Milwaukee) also was performed in six patients. In these patients, MR and CT were compared to determine their relative sensitivities for the detection of intratumoral calcification. Axial 10-mm-thick CT slices from the foramen magnum to the vertex were obtained both before and after administration of IV contrast material (iothalamate meglumine, Conray 60, Mallinckrodt, St. Louis) in each instance.

Results

Of 10 ependymomas, six were infratentorial and four were supratentorial. One subependymoma was supratentorial, the other infratentorial (Table 1). Only three of the 10 ependymomas were entirely intraventricular (cases 4, 5, and 9). Two of the supratentorial ependymomas (cases 8 and 10) were entirely intraparenchymal. Five "transependymal" neoplasms (cases 1–3, 6, and 7) arose within the ventricular system but breached the ependymal lining to invade the surrounding parenchyma (Fig. 1). Both subependymomas (cases 11 and 12) were entirely intraventricular.

MR demonstrated well the routes of extension of the partially or completely intraventricular neoplasms. Three supratentorial tumors (two ependymomas, one subependymoma) extended from the lateral to the third ventricle by traversing the foramen of Monro (Figs. 2 and 3). Four infratentorial ependymomas (cases 3, 4, 6, and 7) extended from the fourth ventricle to the cerebellopontine angle cistern through a

TABLE 1: MR Findings in 12 Patients with Intracranial Ependymoma and Subependymoma

Tumor/Case No.	Age (years)	Sex	Primary vs Recurrent	Location	Consistency	Signal Intensity of Solid Tumor Relative to White Matter			Signal Intensity Heterogeneity	Margins		Edema
						T1W	PDW	T2W		T1W	T2W	
Ependymoma												
1	1.2	F	Primary	IT, T	Solid	−	+	+	Yes	Mod	Well	No
2	3.8	M	Recurrent	IT, T	Solid	−	+	+	No	Poor	Mod	Yes
3	6.2	F	Primary	IT, T	Solid	−	+	+	No	Poor	Mod	No
4[a]	5.3	F	Primary	IT, IV	Solid	=/−	+	+	Yes	Mod	Well	Yes
	6.2		Recurrent	IT, IV	Solid	=/−	+	+	Yes	Mod	Well	Yes
5	9.0	M	Recurrent	ST, IV	Solid	=/−	+	+	Yes	Well	Well	No
6	35.0	F	Recurrent	IT, T	Solid	−	+	+	Yes	Well	Well	No
7[b]	59.0	M	Primary	IT, T	Solid	−	+	+	No	Poor	Well	No
				IT, T	Solid	−	+	+	No	Mod	Well	No
8	8.3	M	Primary	ST, IP	Mixed	NA	+	+	No	Well	Well	No
9	25.4	F	Recurrent	ST, IV	Solid	=/−	+	+	No	Poor	Mod	No
10	37.0	F	Primary	ST, IP	Mixed	=/−	NA	+	No	Poor	Poor	Yes
Subependymoma												
11	37.0	M	Recurrent	ST, IV	Solid	−	+	+	Yes	Well	Poor	Yes
12	55.5	M	Primary	IT, IV	Solid	−	+	+	No	Poor	Well	No

Note.—T1W = T1-weighted images; PDW = proton-density-weighted images; T2W = T2-weighted images; IT = infratentorial; T = transependymal; IV = intraventricular; ST = supratentorial; IP = intraparenchymal; − = hypointense; + = hyperintense; = represents isointense; mixed = solid and cystic components; NA = not available. Margins were moderately well (mod), poorly (poor), or well delineated (well).

[a] Examination was repeated at time of recurrence.

[b] Examination was repeated 12 days after surgery.

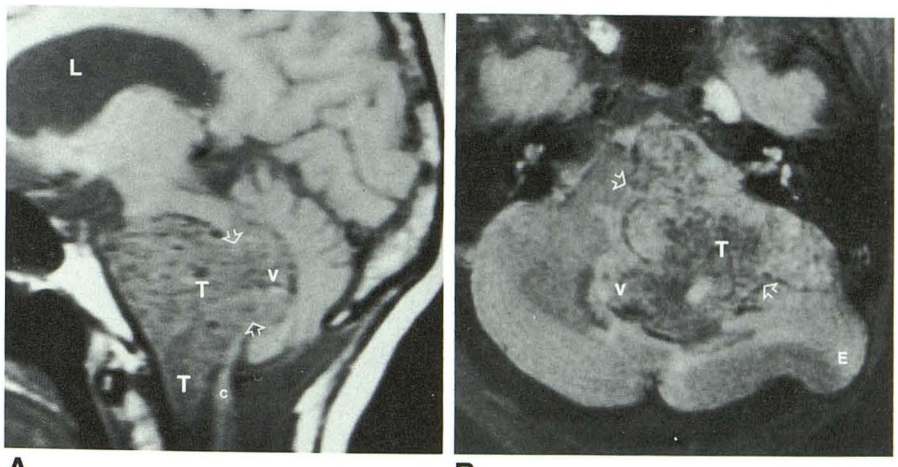

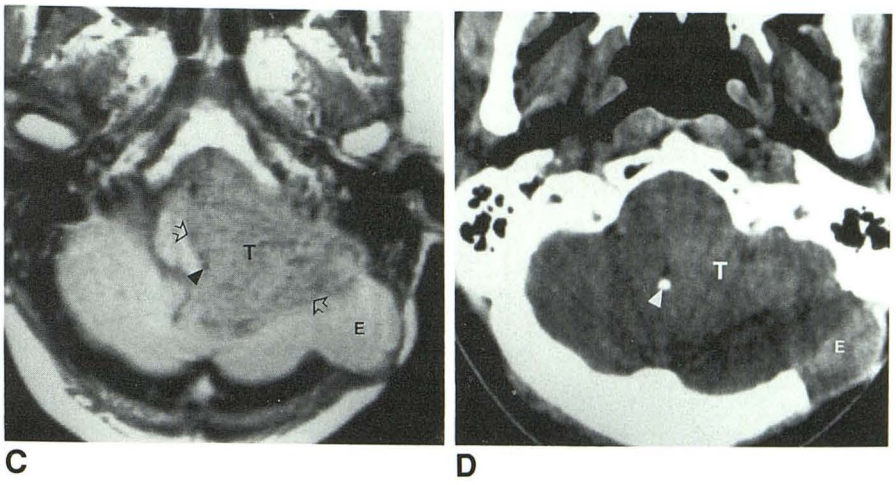

Fig. 1.—Case 6: 35-year-old woman with solid, infratentorial, transependymal ependymoma; postoperative MR studies are at 1.5 T.

***A* and *B*, T1-weighted, 600/25 (*A*), and axial T2-weighted, 2000/70 (*B*), images show tumor (T) arising within fourth ventricle (V) and extending posterolaterally to involve left cerebellar hemisphere and anterolaterally into left cerebellopontine angle cistern via grossly widened lateral recess of fourth ventricle and foramen of Luschka (*arrows*). Tumor extends inferiorly through foramen magnum into upper cervical canal (*A*). Cervical cord (c) is displaced posteriorly by tumor. Lateral ventricle (L) is dilated owing to hydrocephalus. Multiple foci of increased and decreased signal intensity within neoplasm correspond to foci of subacute hemorrhage, hemosiderin, and vessels described in pathology report. Postsurgical encephalocele (E) is present.**

***C* and *D*, T1-weighted image, 800/25 (*C*), corresponds to CT image (*D*). Punctate calcification (*arrowhead*, *D*) at periphery of neoplasm, seen well on CT, was recognized on MR image only in retrospect (*arrowhead*, *C*) as a region of nonspecific hypointensity.**

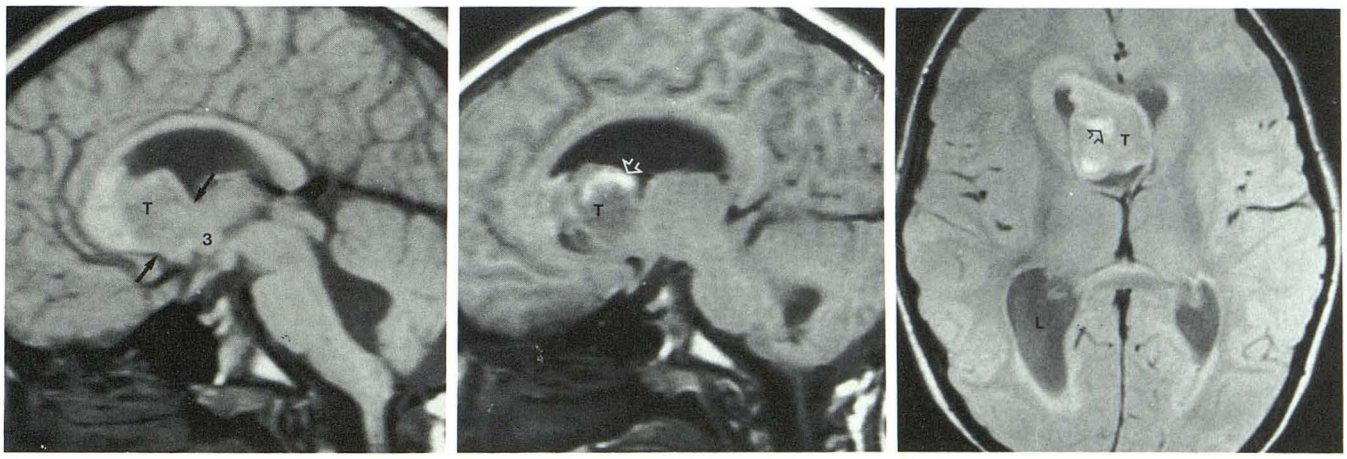

Fig. 2.—Case 5: 9-year-old boy with solid, supratentorial, intraventricular ependymoma.

***A* and *B*, T1-weighted, 600/25 (*A* and *B*), and axial proton-density-weighted, 2000/20 (*C*), postoperative images at 1.5 T show solid neoplasm (T) located within third ventricle (3, *A*) and anterior horns of both lateral ventricles (*C*) traversing foramen of Monro (*solid arrows*). Areas of greatest hyperintensity within tumor (*open arrows*) represent subacute hemorrhage. Dilated lateral ventricles (L) indicate hydrocephalus.**

greatly enlarged lateral recess of the fourth ventricle and foramen of Luschka (Figs. 1, 4, and 9). These four tumors also extended caudally via the foramen of Magendie and foramen magnum, impinging on the upper cervical spinal cord. A subependymoma originating from the fourth ventricle extended superiorly within the aqueduct of Sylvius (Fig. 6). Sagittal and coronal images were important adjuncts to axial images in assessing these routes of tumor spread.

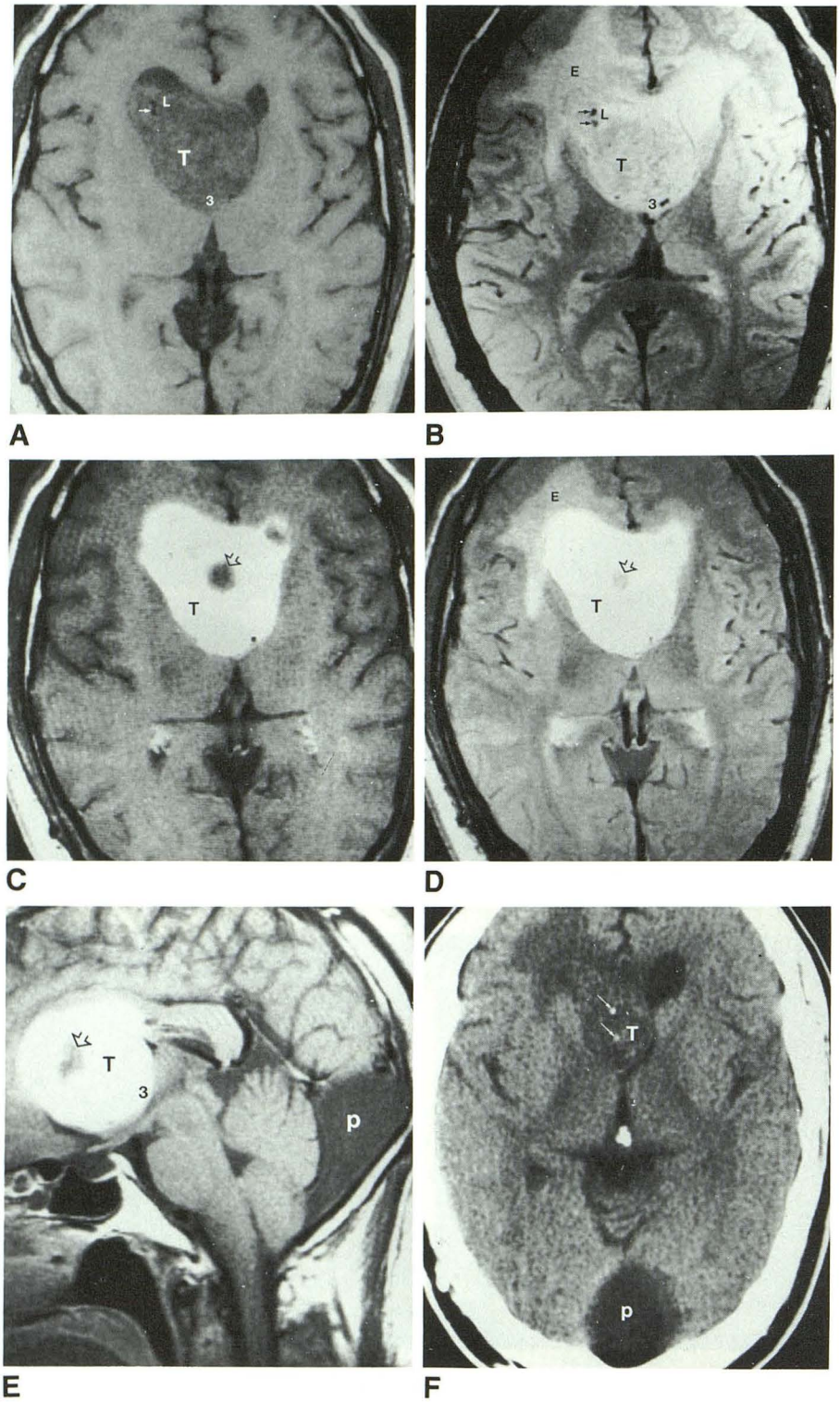

Fig. 3.—Case 11: 37-year-old man with solid, supratentorial subependymoma; postoperative MR studies are at 1.5 T.

***A* and *B*, Axial, noncontrast T1-weighted, 600/25 (*A*), and proton-density-weighted, 2000/25 (*B*), images show solid tumor (T) within lateral (L) and third (3) ventricles traversing foramen of Monro. Two small foci of signal void (*arrows*) within tumor most likely represent vessels. Note that tumor has signal intensity similar to that of edema (E) in forceps minor on long TR image (*B*).**

***C–E*, Axial T1-weighted, 600/25 (*C*), axial proton-density-weighted 1500/30 (*D*), and sagittal T1-weighted, 600/25 (*E*), images after IV Gd-DTPA administration show marked enhancement of tumor. This enhancement clearly demarcates neoplasm from surrounding edema that obscured its margins on precontrast, long TR image (compare *B* and *D*). Central nonenhancing focus likely represents cystic change (*arrows*) not detected on precontrast images. Apparent contrast enhancement in anterior portion of corpus callosum suggests tumor invasion of that structure (*E*). 3 = tumor within third ventricle; p = incidental retrocerebellar arachnoid pouch.**

***F*, Axial CT image. Punctate calcification (*arrows*) within neoplasm were not demonstrated on MR.**

Eight ependymomas and two subependymomas appeared completely solid on MR, whereas two supratentorial ependymomas had both solid and cystic components (cases 8 and 10 [Fig. 7]). Cystic tumor components could be identified on MR as sharply defined, round or oval regions with uniform signal intensity equivalent to that of CSF on all pulse sequences at 0.35 T and 1.5 T. Occasionally, cystic components were slightly hyperintense relative to CSF on long TR images,

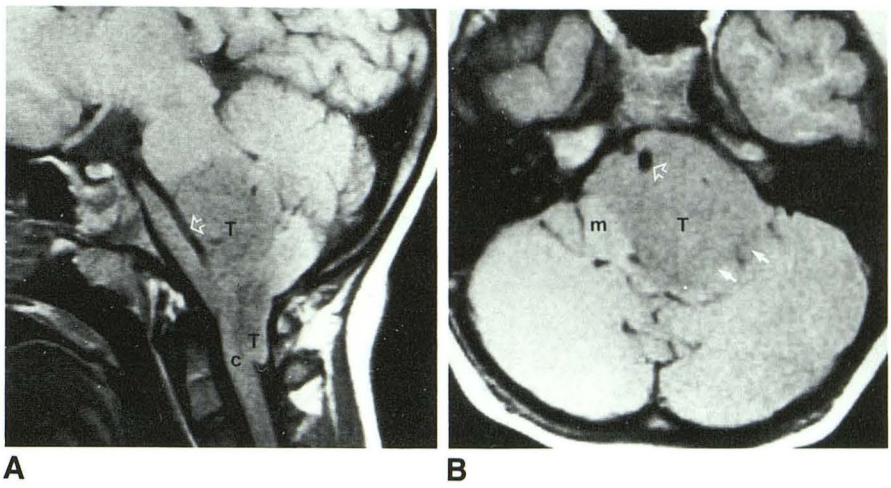

Fig. 4.—Case 3: 6-year-old girl with solid, infratentorial ependymoma.

A and *B*, Sagittal (*A*) and axial (*B*) T1-weighted images, 600/25, at 1.5 T show that neoplasm (T) has homogeneous signal intensity that is less than that of adjacent white matter; tumor encases basilar artery (*open arrows*) and extends into cervical spinal canal via foramen magnum. Cervical cord (c) is displaced anteriorly. Tumor extends from greatly widened left lateral recess of fourth ventricle and foramen of Luschka (*solid arrows*) into left cerebellopontine angle cistern. Medulla (m) is displaced to the right by neoplasm.

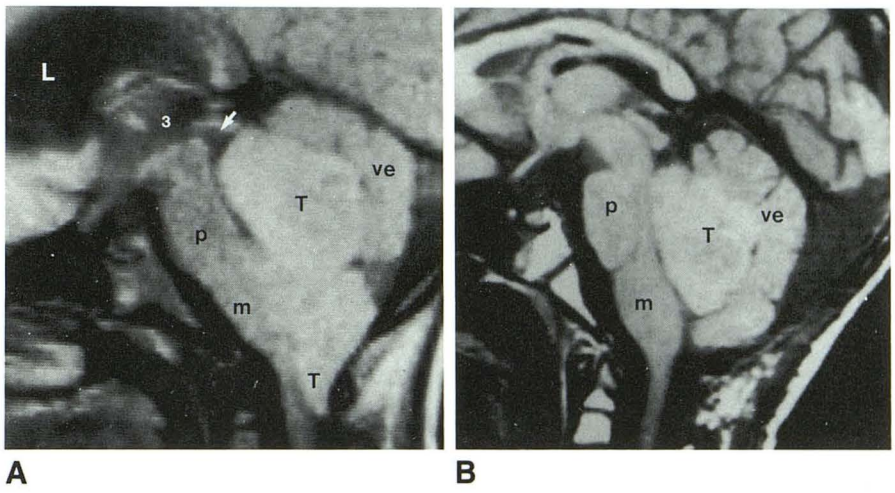

Fig. 5.—Case 4: 5-year-old girl with solid ependymoma of fourth ventricle.

A, Sagittal proton-density-weighted preoperative image, 1500/28, at 0.35 T shows that neoplasm (T) fills fourth ventricle, enters aqueduct of Sylvius (*arrow*), displaces pons (p) and medulla (m) anteriorly, and extends caudally into cervical spinal canal via foramen of Magendie and foramen magnum. Vermis (ve) is uplifted by tumor. Lateral (L) and third (3) ventricles are enlarged owing to hydrocephalus.

B, Sagittal T1-weighted postoperative image, 600/25, at 1.5 T shows recurrence of neoplasm approximately 1 year after biopsy and debulking. Much of extraventricular portion of tumor, particularly that inferior to fourth ventricle, has been removed.

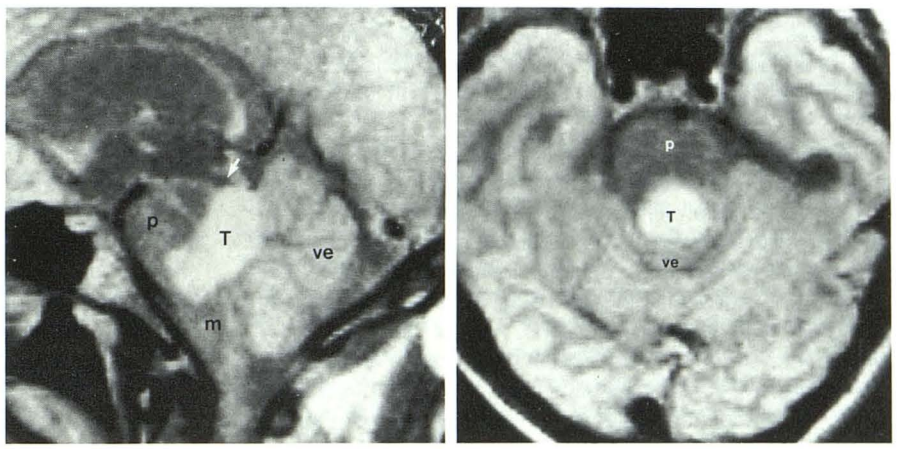

Fig. 6.—Case 12: 55-year-old man with solid infratentorial subependymoma.

A and *B*, Sagittal (*A*) and axial (*B*) proton-density-weighted images 2000/28, at 0.35 T show solid, homogeneous neoplasm (T) within fourth ventricle compressing pons (p) and extending upward into aqueduct of Sylvius (*arrow*). Tumor exhibits typical bright signal intensity relative to white matter on proton-density-weighted image; tumor margins are extremely well defined. ve = vermis; m = medulla.

likely owing to high protein content and restricted flow within the cyst.

Completely solid tumors and the solid components of mixed solid and cystic neoplasms were iso- to hypointense relative to normal white matter (but remained brighter than CSF) on T1-weighted images; solid tumor was hyperintense relative to normal white matter on T2- and proton-density-weighted images (Figs. 3 and 8) in all instances. Compared with CSF, the solid neoplasms were hypo- to hyperintense on T2-weighted images and iso- to hyperintense on proton-density-

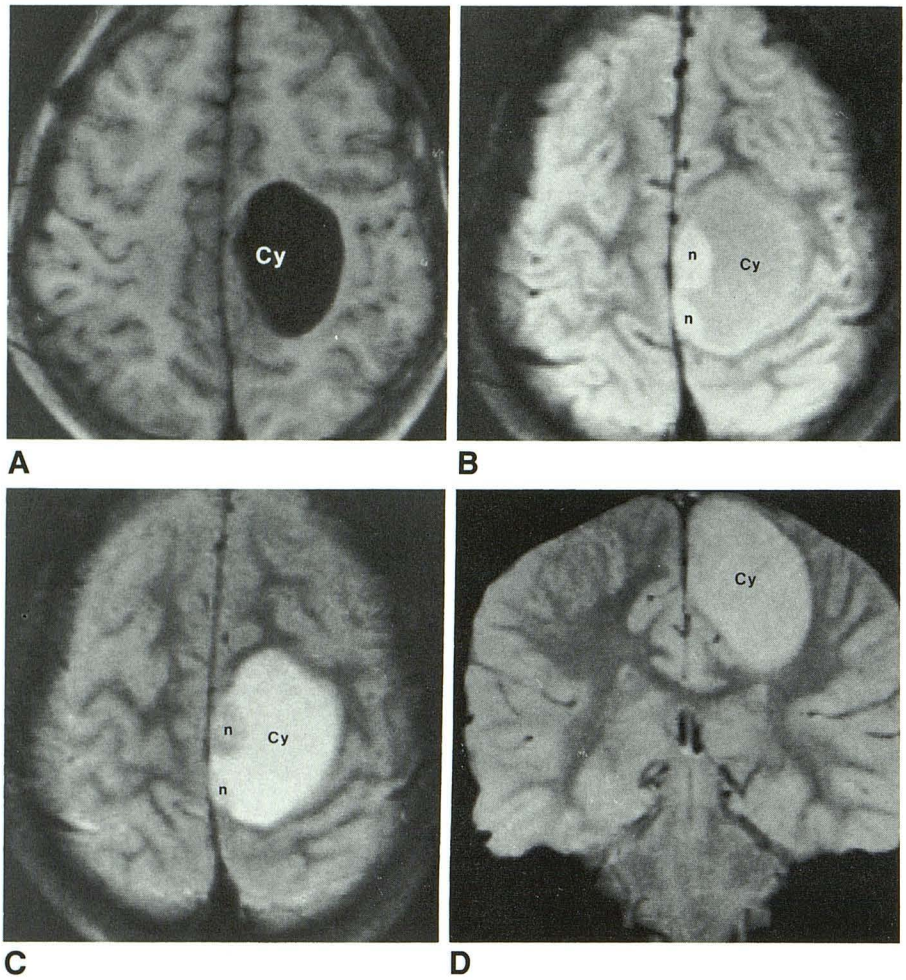

Fig. 7.—Case 8: 8-year-old boy with mixed cystic and solid ependymoma; MR images are at 0.35 T.

***A*, Axial T1-weighted image, 500/30, shows tumor within parenchyma of left cerebral hemisphere, which has a large cystic component (Cy). Signal intensity of fluid is similar to that of CSF.**

***B* and *C*, Axial proton-density-weighted, 2000/30 (*B*), and T2-weighted, 2000/60 (*C*), images at a slightly higher level show tumor nodules (n) in medial wall of cyst (Cy) that are hyperintense relative to white matter. High signal intensity of cyst fluid relative to CSF likely is due to higher protein content and restricted flow within cyst.**

***D*, Coronal partial-flip-angle image, 500/30/30°, clearly depicts intraparenchymal nature of tumor. While supratentorial ependymomas tend to have cystic components, as in this example, this appearance is not specific for ependymomas and may be seen with other gliomas, particularly cystic astrocytoma.**

weighted images. No difference in signal-intensity characteristics was observed between primary and recurrent tumors, and essentially no difference in the signal intensity of solid tumor was noted between images obtained at 0.35 and at 1.5 T.

One patient with a solid ependymoma (case 4) was examined at 0.35 T at initial presentation and at 1.5 T at the time of recurrence (approximately 11 months after initial presentation), which followed surgical debulking, radiation therapy, and chemotherapy (Fig. 5). No significant difference was noted in the signal-intensity characteristics of this neoplasm at the two different field strengths. Another patient (case 7) was imaged at 1.5 T at both initial presentation and 12 days after surgery. Both examinations showed a solid infratentorial tumor of homogeneous signal intensity; the bulk of the neoplasm was within a markedly enlarged left lateral recess of the fourth ventricle and foramen of Luschka. The signal-intensity characteristics of this neoplasm were identical on both studies.

Solid portions of five tumors (four ependymomas, one subependymoma) demonstrated signal heterogeneity; that is, scattered foci of increased or diminished signal intensity compared with surrounding tumor tissue on T1-weighted and/or T2-weighted images. This finding was correlated with pathologic and surgical reports. Regions of recent (1–4 weeks) and old (>1 month) hemorrhage, hemosiderin deposition, necrosis, calcification, or tumor vascularity accounted for heterogeneous signal intensity (Figs. 1, 2, and 5).

Hypointensity possibly representing calcification was not recognized prospectively by MR in any of the lesions. Nevertheless, CT examinations available in six patients (cases 2, 3, 6, 8, 10, and 11) revealed that four (cases 6, 8, 10, and 11) had punctate (<5 mm), intratumoral foci of calcification (Fig. 3). In retrospect, a focus of decreased signal intensity within one ependymoma (case 6) most likely corresponded to a punctate calcification demonstrated by CT (Fig. 1).

Parenchymal swelling accompanying high signal intensity on long TR images, likely representing edema, either completely or partially surrounded four tumors. Edema accompanied both intraventricular and intraparenchymal neoplasms. In case 2, examined at the time of postsurgical recurrence, we were unable to differentiate between edema and postoperative changes. After IV administration of Gd-DTPA in case 11, the tumor (subependymoma) tissue demonstrated intense, diffuse enhancement, more clearly delineating it from surrounding edema on proton-density- and T2-weighted im-

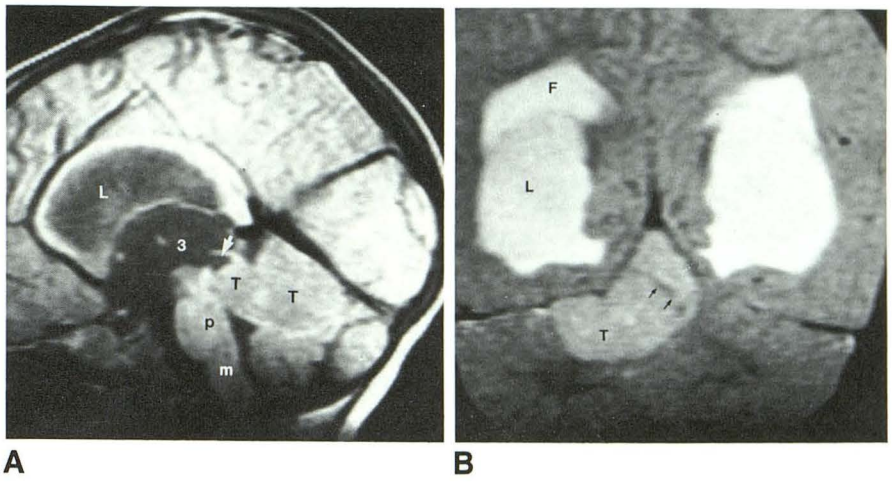

Fig. 8.—Case 1: 1-year-old girl with solid ependymoma within right cerebellum and vermis; MR images are at 1.5 T.

***A*, Sagittal T1-weighted image, 900/20, shows typical hypointensity of tumor (T) relative to white matter (compare with corpus callosum). Tumor abuts fourth ventricle and extends into and widens aqueduct of Sylvius (*arrow*). Dilatation of third (3) and lateral (L) ventricles indicates hydrocephalus. p = pons; m = medulla.**

***B*, Coronal T2-weighted image, 2800/80, shows typical hyperintensity of tumor relative to white matter. Tumor has distinct margins. Linear signal void coursing through superior aspect of mass (*arrows*) likely represents an encased vessel. High signal intensity (F) adjacent to dilated lateral (L) ventricles suggests transependymal flow of CSF.**

ages (Fig. 3). A nonenhancing focus within the tumor likely represented cystic change, which was described in the pathology report.

Tumor margins with surrounding parenchyma were delineated well on T2-weighted images in nine instances, moderately well in three, and poorly in two. On T1-weighted images, tumor margins with surrounding normal or edematous parenchyma were well delineated in four examinations, moderately well delineated in four, and poorly delineated in six instances. In case 10, surrounding edema completely obscured the margins of the tumor on all pulse sequences. The margins of the tumors, when visible, were most distinct on T2-weighted images. The differentiation of neoplasm from surrounding brain parenchyma on T1-weighted images was significantly improved after administration of Gd-DTPA in case 7. The tumor exhibited moderate, heterogeneous enhancement.

The displacement or encasement of normal vasculature and the presence of tumor vascularity were well demonstrated in 10 examinations (nine patients) (Figs. 1, 4, and 8). Encasement of normal vessels occurred in four infratentorial ependymomas (cases 1, 3, 6, and 7). Vessels involved included the basilar artery, vertebral artery, and petrosal and vermian veins. Pathologic and surgical reports in cases 3 and 6 verified vessels traversing the tumors. Three supratentorial lesions (cases 5, 9, and 11) displaced internal cerebral, subependymal and anterior caudate, or thalamostriate veins. In case 10, the surgical report corroborated the MR finding of numerous capsular vessels surrounding a supratentorial ependymoma. Two infratentorial ependymomas displaced a prominent vascular structure likely representing the vein of the lateral recess of the fourth ventricle (see Fig. 9 and Discussion).

Discussion

Few prior descriptions are available on the MR appearance of intracranial ependymoma. One report mentioned the cystic nature of a posterior fossa ependymoma without further characterization [5]. Another report listed two patients with ependymoma; the cystic component of one of the tumors had longer T1 and T2 relaxation times than did the solid component [7]. MR performed in one of 12 subependymomas demonstrated a midline posterior fossa tumor with a long T2 [9].

In our series, solid ependymomas and the solid portions of mixed solid and cystic ependymomas were hypo- to isointense compared with white matter on T1-weighted images and hyperintense on T2-weighted images, similar to other intracranial tumors [11, 12]. The signal intensity of cystic tumor components was similar to that of CSF on T1-weighted images and iso- to hyperintense relative to CSF on T2-weighted images. Cystic portions were present in two supratentorial ependymomas; unlike infratentorial ependymomas, supratentorial lesions tend to have cystic components [1].

The two patients in our series with subependymomas had similar clinical and imaging features including later age of presentation (37 and 55.5 years of age) than the patients with ependymoma, epicenter within the lateral or fourth ventricle, and predominantly homogeneous hyperintensity relative to surrounding brain parenchyma on T2-weighted images. At pathology, subependymomas are benign, solid subependymal nodular masses that usually extend into the ventricle. Most often they are found incidentally at autopsy [9]. The subependymomas in our series could not be distinguished from ependymomas by signal-intensity differences, consistency, or location. The differentiation of these two tumors was accomplished histologically (Fig. 10).

Signal heterogeneity within the solid tumors in our series had various etiologies. Subacute (1–4 weeks) hemorrhage accounted for foci of hyperintensity on both T1- and T2-weighted images owing to the presence of dilute methemoglobin outside of lysed RBCs [14, 15]. Regions of diminished signal intensity relative to white matter on both T1- and T2-weighted images represented hemosiderin deposition, necrosis, vessels, and calcification. In case 11, cystic change was suggested by a nonenhancing area within the neoplasm after administration of Gd-DTPA.

Tumor vascularity and encasement or displacement of normal vessels were well demonstrated by MR; the signal void within these serpentine structures afforded excellent contrast with adjacent brain parenchyma and tumor. Of particular

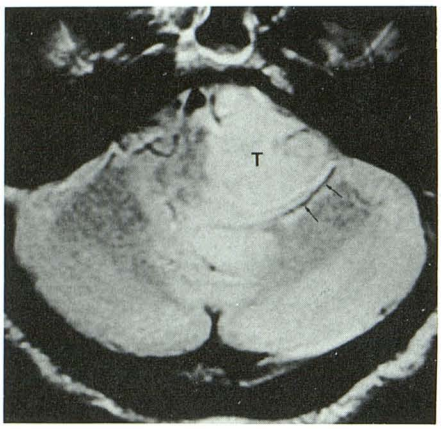

Fig. 9.—Case 7: 59-year-old man with solid, infratentorial ependymoma. Axial proton-density-weighted image, 2800/30, at 1.5 T shows tumor (T) expanding left lateral recess of fourth ventricle and foramen of Luschka. Vascular structure (*arrows*) adjacent to posterior aspect of tumor likely represents displaced vein of lateral recess [10].

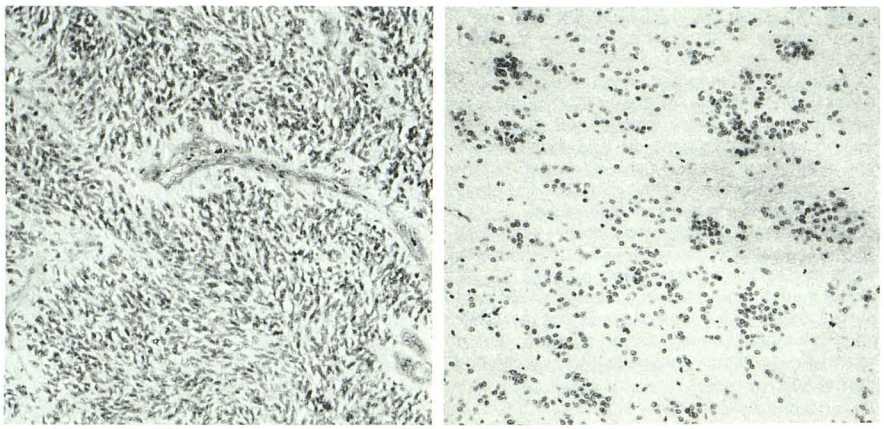

Fig. 10.—*A* and *B*, Ependymoma (*A*) and subependymoma (*B*). Whereas ependymoma is characterized histologically by ependymal perivascular pseudorosette with clear zones of elongated cytoplasmic processes around blood vessels, subependymoma shows randomly scattered clusters of nuclei, reminiscent of those of normal ependyma, within dense fibrillary background [13].

interest, two infratentorial ependymomas displaced a prominent vascular structure that had the expected course of the vein of the lateral recess of the fourth ventricle [10]. This vein originates from the transverse and lateral supratonsillar veins in the anterolateral aspect of the superior pole of the cerebellar tonsil. The vein of the lateral recess then courses forward and laterally (immediately behind and below the lateral recess of the fourth ventricle) to the cerebellopontine angle, runs over the brachium pontis, and joins other veins to form the petrosal vein. As a marker of the posterior border of the lateral recess of the fourth ventricle, the vein of the lateral recess is displaced posterolaterally by tumors that expand the fourth ventricle and its lateral recesses [10]. The superior visualization of vessels at high field strength in one patient imaged at 0.35 T and 1.5 T likely was due to thinner slices and improved spatial resolution.

Four (40%) of 10 ependymomas in our study were supratentorial, while six (60%) of 10 were infratentorial. One of the two subependymomas was supratentorial; the other was infratentorial. Several series report that 30–40% of intracranial ependymomas are supratentorial in origin [2, 3]. Whereas supratentorial ependymomas tend to be parenchymal, infratentorial ependymomas usually are intraventricular [1]. It has been postulated that ependymal rests outside of the ventricular lining may give rise to extraventricular ependymomas [2]. In our series, three of 10 ependymomas were intraventricular, two were intraparenchymal, and five were transependymal (extending from CSF spaces into the parenchyma). Of the four supratentorial neoplasms, two were parenchymal and two intraventricular. Five of six infratentorial tumors were transependymal and one was completely intraventricular; therefore, all infratentorial ependymomas were at least partially intraventricular.

The multiplanar imaging capability of MR was valuable in assessing the location and routes of extension of ependymomas. Particularly useful were sagittal images of the posterior fossa tumors. The sagittal plane demonstrated best the walls of the fourth ventricle and tumor within it or extending from it. The extension of tumor from the fourth ventricle laterally into the cerebellopontine angle via the lateral recess of the fourth ventricle and foramen of Luschka in three patients and the downward extension into the cisterna magna and cervical spinal canal through the foramen of Magendie and foramen magnum in four patients were demonstrated well on sagittal and axial images. The propensity of ependymomas to "ooze out of the foramina" has been described previously in the surgical pathology literature [13].

Calcifications noted in three of five ependymomas and in one subependymoma on CT were not appreciated prospectively on MR in our series. In retrospect, a focal (<5 mm) region of hypointensity noted within one tumor did correspond to the presence of calcification on CT. Calcification occurs in approximately 50% of supratentorial and 25–50% of infratentorial ependymomas [1]. Previous authors found that focal calcifications accompanying many disease processes are commonly missed by MR [16]; in such instances it is likely that mobile protons in soft tissues within the interstices of the calcification generate sufficient signal to predominate over the nonmobile protons of the calcification, which generate little signal [16]. Recently, MR with gradient-echo acquisition proved more sensitive than spin-echo MR for the detection of intraparenchymal calcification, which appeared as regions of low signal intensity [17].

Intratumoral bleeding occurs infrequently in ependymomas, with prevalences of 0–13% in two series [1, 2]. Findings compatible with subacute hemorrhage within the neoplasm were seen in two patients in our series with recurrent ependymomas (cases 5 and 6) and were verified in the pathology report in one of them. Because these patients were imaged 5 and 2 years, respectively, after surgery, the bright foci of subacute hemorrhage most likely were due to the natural course of the tumor.

On noncontrast MR, tumor boundaries were best recognized on T2-weighted images and less well delineated on T1-weighted images. In one instance (case 10), surrounding parenchymal edema completely obscured the margins of the neoplasm on T1-, proton-density-, and T2-weighted sequences. MR was performed after administration of Gd-DTPA in two patients. In one instance, enhancing subependymoma was better delineated from surrounding hypointense edema on proton-density- and T2-weighted images. In the other patient, the enhancing tumor on post–Gd-DTPA T1-weighted images had more distinct margins with respect to surrounding brain parenchyma than on the preconstrast T1-weighted images. Nevertheless, it is important to emphasize that isolated tumor-cell infiltration may exist outside the margins of contrast enhancement [18].

The differential diagnosis of intracranial ependymoma and subependymoma depends on the location of the tumor and the age of the patient. Other supratentorial, intraventricular neoplasms in children include choroid plexus papilloma, a multilobular, solid mass; colloid cyst, characteristically a unilocular cystic tumor in the third ventricle; and astrocytoma, particularly the subependymal giant cell astrocytoma, which is usually associated with tuberous sclerosis [19]. Craniopharyngioma may extend upward into the third ventricle [20]. Moreover, in adults one must consider intraventricular meningioma and metastatic carcinoma to the ependyma [21]. Medulloblastoma, choroid plexus papilloma, and astrocytoma may present as fourth ventricular masses in children [2, 19]. Metastases [21] and less commonly dermoid and epidermoid cysts may also involve the fourth ventricle in adults [22]. When confronted with a supratentorial, intraparenchymal mass (seen in two ependymomas in our series), additional lesions that should be considered include astrocytoma, undifferentiated glioma, metastatic carcinoma, and oligodendroglioma [1, 21].

In summary, signal-intensity characteristics do not distinguish ependymoma or subependymoma from other intracranial gliomas; the intra- or periventricular location and morphology of the former seem to be more reliable distinguishing features. The clinical setting and MR appearance of subependymomas, while not completely specific, are suggestive of the histology. Tumor-associated calcification was not readily detected on MR. Coronal and sagittal images were helpful in defining intraventricular tumor and routes of extension within and outside of CSF spaces. Encasement and displacement of normal vessels and tumor vascularity are well shown by MR. Gd-DTPA shows promise in the evaluation of intracranial ependymoma by helping to distinguish enhancing tumor from nonenhancing edema and surrounding normal brain parenchyma.

ACKNOWLEDGMENTS

We thank Robert Prager, Kenneth Albertson, and Hector James for providing us with some of the patients evaluated in this report and Marjorie Grafe for the histological specimen photographs.

REFERENCES

1. Armington WG, Osborn AG, Cubberley DA, et al. Supratentorial ependymoma: CT appearance. *Radiology* **1985**;157:367–372
2. Naidich TP, Zimmerman RA. Primary brain tumors in children. *Semin Roentgenol* **1984**;19:100–114
3. Van Tassel P, Lee Y, Bruner JM. Supratentorial ependymomas: computed tomographic and pathologic correlations. *J Comput Tomogr* **1986**;10:157–165
4. Gadian DG, Payne JA, Bryant DJ, Young IR, Carr DH, Bydder GM. Gadolinium-DTPA as a contrast agent in MR imaging—theoretical projections and practical observations. *J Comput Assist Tomogr* **1985**;9(2):242–251
5. Lee BCP, Kneeland JB, Deck MD, Cahill PT. Posterior fossa lesions: magnetic resonance imaging. *Radiology* **1984**;153:137–143
6. Randell CP, Collins AG, Young IR, et al. Nuclear magnetic resonance imaging of posterior fossa tumors. *AJR* **1983**;141:489–496
7. Han JS, Benson JE, Kaufman B, et al. MR imaging of pediatric cerebral abnormalities. *J Comput Assist Tomogr* **1985**;9(1):103–114
8. Press GA, Hesselink JR. MR imaging of cerebellopontine angle and internal auditory canal lesions at 1.5 T. *AJNR* **1988**;9:241–251
9. Jooma R, Torrens MJ, Bradshaw J, Brownell B. Subependymomas of the fourth ventricle. *J Neurosurg* **1985**;62:508–512
10. Huang YP, Wolf BS. The vein of the lateral recess of the fourth ventricle and its tributaries. *AJR* **1967**;101:1–21
11. Lee BCP, Kneeland JB, Cahill PT, Deck MDF. MR recognition of supratentorial tumors. *AJNR* **1985**;6:871–878
12. Komiyama M, Yagura H, Baba M, et al. MR imaging: possibility of tissue characterization of brain tumors using T1 and T2 values. *AJNR* **1987**;8:65–70
13. Burger PC, Vogel FS. *Surgical pathology of the nervous system and its coverings*, 2nd ed. New York: Wiley, **1982**:302–315
14. Gomori JM, Grossman RI, Goldberg HI, Zimmerman RA, Bilaniuk LT. Intracranial hematomas: imaging by high field MR. *Radiology* **1985**;157:87–93
15. Grossman RI, Gomori JM, Goldberg HI, et al. MR imaging of hemorrhagic conditions of the head and neck. *RadioGraphics* **1988**;8(3):441
16. Oot RF, New PJF, Pile-Spellman J, Rosen BR, Shoukimas GM, Davis KR. The detection of intracranial calcifications by MR. *AJNR* **1986**;7:801–809
17. Atlas SW, Grossman RI, Hackney DB, et al. Calcified intracranial lesions: detection with gradient-echo-acquisition rapid MR imaging. *AJNR* **1988**;9:253–259
18. Johnson PC, Hunt SJ, Drayer BP. Human cerebral gliomas: correlation of postmortem MR imaging and neuropathologic findings. *Radiology* **1989**;170:211–217
19. Sanford RA, Laurent JP. Intraventricular tumors of childhood. *Cancer* **1985**;56:1795–1799
20. Tew JM, Feibel JH, Sawaya R. Brain tumors: clinical aspects. *Semin Roentgenol* **1984**;14(2):115–128
21. Rosai J. *Ackerman's surgical pathology*, 7th ed. St. Louis: Mosby, **1989**:1713–1771
22. Yu WTC, Berloon TJ, Jacoby CG, Schultz DH. MR of fourth-ventricular epidermoid tumors. *AJNR* **1988**;9:794–796